Modelling of a DC-DC Boost Converter in QRM and Design of Neural Network-Based Nonlinear Control

Zhi Li[1,2], Benjamin Schwabe[2], Lorenzo Servadei[1,3], Robert Wille[1]

Abstract— Boost converters are a crucial component in power conversion systems, often operated in quasi-resonant mode (QRM) to reduce switching losses and enhance efficiency for medium and low power level applications. However, traditional modelling approaches have difficulties in balancing simulation speed and accuracy, particularly during transient phases. Moreover, conventional linear control schemes such as PI control have limitations in fast transient regulation.

In this paper, a state machine-based model is proposed and tested. Compared to Simscape model in MATLAB/Simulink, the proposed modelling method shows high accuracy in output voltage both in steady state and transient phase. Furthermore, a neural network-based nonlinear control scheme has been designed to optimize the transient response and is compared to a tuned PI controller.

I. Introduction

Due to their simple topology and capability of voltage stepping up, boost converters are extensively applied in power conversion systems, for instance, in power factor correction units [1], battery-powered systems [2], and photovoltaic solar systems [3]. Considering the energy efficiency and the inductor volume, boost converters usually operate in discontinuous conduction mode (DCM) or even quasi-resonant mode (QRM) for medium and low power level applications [2], [3].

For control design and tuning, averaged models are usually used without considering the resonant phenomenon and the valley switching modulator [4]. However, the control of switch-on time with variant switching frequency cannot be represented by these modelling methods. In addition, model averaging for different operating conditions is needed that makes the control design complicated and time-consuming. Thus, modelling with consideration of valley switching and fast design flow is significant necessary for investigating control design and tuning for boost converter in QRM.

In terms of control schemes, traditional proportional-integral-derivative (PID) controllers are usually faced with the limitation of balancing fast transient response and high robustness. Inspired by the structure of PID controllers, a recurrent neural network architecture has been developed for nonlinear control, and the proposed architecture can be further extended [5]. The nonlinearity of neural network-based controllers empowers different dynamic behaviors at various operating points.

In this work-in-progress paper, a new modelling method is proposed for DC-DC boost converters operating in QRM. Moreover, a neural network-based nonlinear controller is introduced for improving boost converter control.

[1]Chair for Design Automation, Technical University of Munich, Munich, Germany.
[2]Infineon Technologies AG, Munich, Germany.
[3]Sony AI, Zurich, Swizerland.
Zhi.Li@tum.de;
Benjamin.Schwabe@infineon.com
Lorenzo.Servadei@sony.com
Robert.Wille@tum.de

II. Modelling of DC-DC Boost Converter and the Control Loop Circuit

Considering the effect of the equivalent series resistance (ESR) of the input inductor and output capacitor, as well as the effect of parasitic capacitance of the metal-oxide-semiconductor field-effect transistor (MOSFET), a model in Simscape blocks and a model represented by a state machine are built for assisting control design and verifying the control performance.

A. Modelling of a DC-DC Boost Converter in QRM with Simscape Blocks

A boost converter with component parameters listed in Table I is modelled in Simulink. Non-critical components and circuits are omitted for simplification, for instance, the drain-source current measurement and protection circuit.

TABLE I
Boost Converter Parameters

Parameter	Symbol	Value
Input voltage	V_{in}	36V-48V
Output voltage	V_{out}	48V-60V
Voltage ripple	ΔV_{out}	2.5%
Transformer ratio	$N_{L1} : N_{aux}$	10:1
Inductance	L_m	470μH
Inductor DC resistance	R_{L1}	225$m\Omega$
Output capacitance	C_1	56μF
Capacitor ESR	R_{C1}	0.014$m\Omega$
MOSFET drain-source on resistance	$R_{\text{ds(on)}}$	280$m\Omega$

Building blocks of Simulink-Simscape Library are used to model the DC-DC boost converter in QRM. A diagram including the boost converter circuit and the control loop is displayed in Fig.1. The inductor is modelled as an ideal transformer with an auxiliary-winding ratio of 10:1. A zero-crossing detection (ZCD) circuit is adopted for modulating the switch drive signal. The MOSFET switch is modelled by an ideal MOSFET

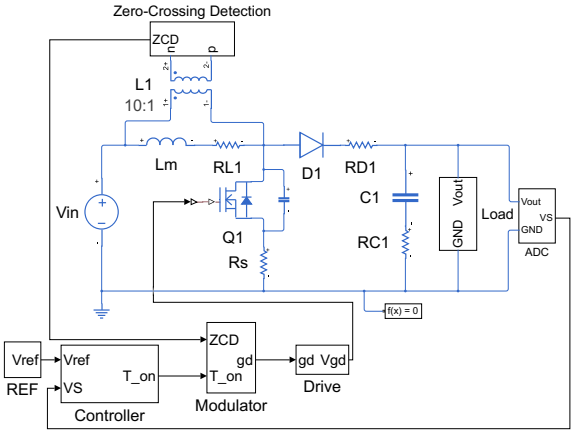

Fig. 1. Simulink diagram of a boost converter and its control loop.

block with drain-to-source on resistance $R_{\mathrm{ds(on)}}$. The parasitic capacitance over drain-to-source poles of the MOSFET, C_{ds}, is estimated by (1) using the measured LC resonant period T_{res} in real hardware.

$$T_{\mathrm{res}} = 2\pi\sqrt{L_m C_{\mathrm{ds}}} \tag{1}$$

With the modelled parasitic capacitor, resonant phenomenon can be observed after the inductor demagnetizes. The power loss of the MOSFET switch is minimized by valley switching strategy, which turns on the MOSFET only at the valley point of the drain-to-source voltage V_{ds}. This paper presents one feasible valley switching modulator in Fig.2.

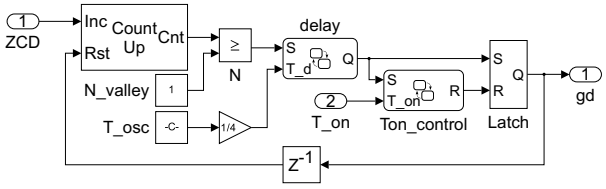

Fig. 2. Simulink Diagram of boost control modulator for QRM valley switching.

This modulator contains two input ports connecting respectively to the control output and to the ZCD block. When the on-time threshold (T_{on}) is reached, a timer in Ton_control block is triggered and resets the Latch, and the output signal gd turns zero for switching-off the MOSFET. Following that a counter accumulates the number of ZCD until it reaches valley number threshold. A comparator N outputs 1 to the latch after $T_{\mathrm{res}}/4$ and outputs a switching-on signal.

This modelling method gives advantage to simulating the boost converter in QRM with valley switching, and the threshold valley number can be determined by the control output. In the following discussion, we consider high relative output power cases and the valley threshold is fixed as one, and only the regulation of on-time is studied.

B. Modelling of Boost Converter and Modulator with a State Machine

Inspired by the work of [6] and the working principle of boost converters, a state machine-based modelling approach is proposed and shown in Fig.3 to represent the boost converter model operating in QRM.

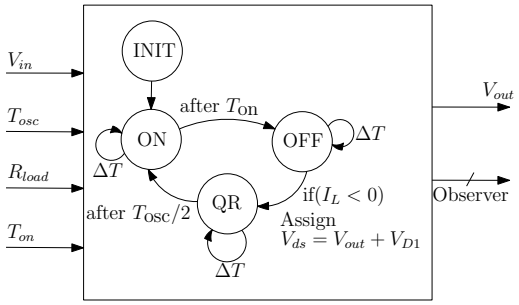

Fig. 3. Diagram of boost converter modelled in a state machine.

The model has four states and three transitions. Initial values are calculated once in the initial (default) state. After the simulation starts, it transits directly to the ON state without condition. In the ON state, the input inductor is magnetized and the output capacitor is discharged. After T_{on} the MOSFET is switched off, and the state machine transits to OFF, when the boost diode is conducted, the inductor is demagnetized, and the output capacitor is charged. Due to the MOSFET's parasitic effect, the converter operates in a quasi-resonant state QR after switching off. The QR state starts when the inductor current drops below zero, and lasts for $T_{\mathrm{res}}/2$ seconds before transiting back to ON. In each of the operating states, the current and voltage of each component are updated every ΔT, which is in this paper $0.1\mu s$.

Assume that the inductor and the capcitor are linear components for simplicity. The current-voltage relationship equations in differential form can be approximated by time-discretized form in a short interval, which are given in (2).

$$\begin{aligned} I_{L1}^{k+1} &= I_{L1}^{k} + \frac{V_{L1}^{k}}{L_1}\Delta T \\ V_{C1}^{k+1} &= V_{C1}^{k} + \frac{I_{C1}^{k}}{C_1}\Delta T \end{aligned} \tag{2}$$

There the superscript k represents the k-th iteration with a step size of ΔT. The state machine block also has the same sample rate ΔT.

C. Comparison Between the Simscape Model and the State Machine Model

To verify the accuracy of the state machine model, its output voltage is compared to that of the Simscape model by operating the converter with the same on-time T_{on} in an open loop. The maximum step size is 1e-7s, relative error tolerance is 1e-6, and the solver is set as daessc.

Three transient behaviors are tested using step functions in a single simulation:

- load resistor changes from 100Ω to 50Ω at 20ms,
- input voltage increases from 36V to 48V at 40ms, and
- on-time increases from 25μs to 30μs at 60ms.

The result is illustrated in Fig.4. The three middle subplots are the zoomed-in view at each transient stage.

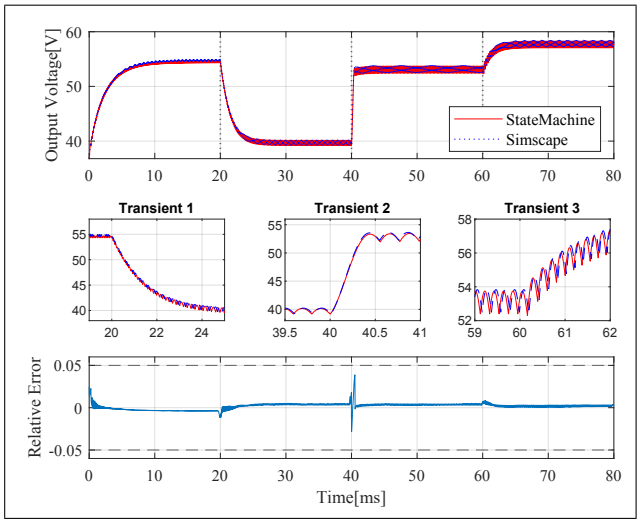

Fig. 4. Step response comparison between Simscape model and state machine model with reference transient, control effort transient, and load transient.

It is observed from the figure that the result of using state machine model is comparable to that of using the Simscape model. Relative error is below 5% during transient stages and is below 2% during steady state.

MATLAB functions tic, toc and timeit[1] are used for simulation time comparison. The simulation time comparison results are listed in Table II. Different stop times are compared.

TABLE II
Averaged simulation time comparison

Stop Time [s]	Modelling Method	Execution Time [s]
0.01	Simscape model	11.8078
0.01	Our method	0.5156
0.1	Simscape model	99.4320
0.1	Our method	2.2836
0.5	Simscape model	509.2744
0.5	Our method	9.7335

The results show that simulations with the proposed state machine modelling method consume less than 10% time of the simulations with the Simscape model. Moreover, the state machine model supports both fixed-step solvers and variant-step solvers, although the state machine and the controller have fixed sample rates. For nonlinear component parameters, it is convenient to extend our modelling method by setting parameters depending on additional input ports. Hence, the state machine model can be used for control design and parameter tuning.

[1]Unlike tic and toc, timeit calls the function multiple times.

III. Neural Network-Based Nonlinear Controller Design and Performance Comparison

A. Design of Neural Network Controller

Inspired by the work of [5], a neural network control scheme is proposed and the principle diagram is shown in Fig.5, composed of a PI layer and a nonlinear activation layer. The activation layer is realized by linear combination of n rectified linear units (ReLUs) with n biases b_k and gains w_k, $k \in [1, 2, \ldots, n]$. The output of each ReLU is connected to a sum neuron.

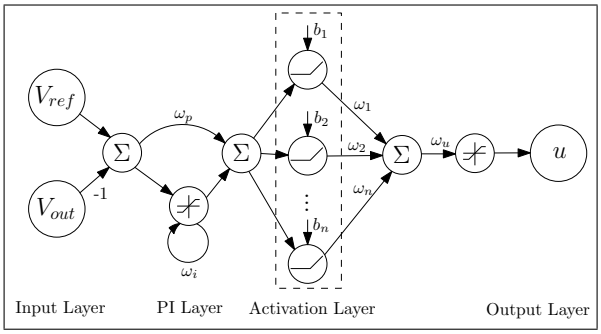

Fig. 5. Neural network-based nonlinear control scheme with a PI layer and a ReLU activation layer.

The PI layer parameters are initialized with Ziegler-Nichols method [8] and the ReLU layers are initialized by unit gains and uniformly distributed biases. The recurrent structure achieves an integral function with a gain of w_i, and the other path in parallel has a proportional gain of w_p. Given the target reference output voltage V_{ref} and the real output voltage V_{out}, the PI layer output u_{PI} is calculated in discrete-form by (3),

$$\begin{aligned} e[k] &= V_{ref}[k] - V_{out}[k], \forall k \in \mathbb{N} \\ u_{\text{PI}}[0] &= w_p e[0] \\ u_{\text{PI}}[k] &= w_p e[k] + w_i u_{\text{PI}}[k-1], \forall k \in \mathbb{N}^+, \end{aligned} \tag{3}$$

and the output of each ReLU is computed by (4),

$$r_k = \max\{0, u_{\text{PI}} - b_k\}, \forall k \in \{1, 2, \ldots, n\}. \tag{4}$$

The neural network controller's output is denoted as u and is calculated by (5).

$$u = w_u \sum_{k=1}^{n} w_k r_k(x) \tag{5}$$

where w_u is the output gain.

The overall controller has a sample time of T_s, greater than the step size of the proposed state machine-based model, ΔT. Given the design in neural network, the gains and biases can be further trained using back-propagation-like methods with prescribed control targets, such as the work in [7]. As is discussed in work [5],

reinforcement learning method can be used for training the parameters. The update algorithm is designed depending on the optimization target. Boundary conditions are considered to satisfy the voltage ripple requirement and the limit of switching frequency, as well as the bandwidth and phase margin requirement of the entire control loop.

B. Performance Comparison Between PI Control and Neural Network-Based Nonlinear Control

Due to additional requirement of noise filters, the derivative component of a PID controller is not used in the following discussion, which is also common in industrial applications of boost converters.

In this section, two neural network controllers (abbreviated as NN controllers) are selected, and the performance is compared to that of a well-tuned PI controller using transient simulation.

Instead of applying the control signal directly from the PI controller, the activation layer of the NN controller performs a nonlinear mapping of the control effort. The gain factor is therefore rescheduled according to the PI layer output. The control effort is amplified only when the PI layer output is high, which means the real-time error and/or accumulated error is high.

The following test conditions are fulfilled: the input voltage is 36V, while the target output voltage changes from 48V to 52V at 25ms, then from 52V to 56V at 45ms, both with a slew rate of 4kV/s. The load resistance changes during the steady state of each voltage level drops from 100Ω to a low value, which is assigned such that the peak power is about 50W. The slew rate of the resistance change is around $5k\Omega/s$. The results are shown in Fig.6.

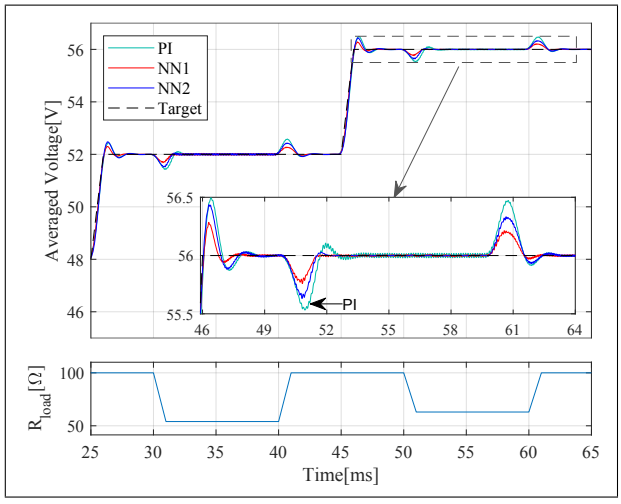

Fig. 6. Compared with the PI controller, the neural network controllers achieve faster energy delivery without causing high overshoot.

The above subplot shows four curves including the target output voltage (black, dashed line), real output voltage with NN controller 1 (red) and NN controller 2 (blue), and the real output voltage with the PI controller (cyan). All the data is averaged and the ripple is smoothed out to focus on the trend. The subplot below shows the variant load resistance.

It can be concluded that the NN controllers can achieve fast energy delivery and enable a faster voltage recovery during the load transient phases. Moreover, the undershoot caused by load transient behavior and the overshoot caused by reference voltage change are lower compared to traditional PI controllers.

IV. Conclusion and Outlook

This work-in-progress paper presents a novel modelling method for DC-DC boost converters operating in QRM using state machine along with the control loop circuit. The proposed modulator circuit can generate a driving signal based on the threshold on-time and desired valley numbers, making it an efficient solution for QRM operations using ZCD mechanisms. The developed state machine model is shown to achieve accuracy comparable to Simscape models, while it offers the benefit of shorter simulation time and can accelerate parameter tuning. The proposed neural network-based nonlinear controllers have demonstrated the ability to achieve faster step responses with lower overshoot or undershoot, outperforming traditional PI controllers.

Future studies will focus on optimizing the training process for the neural network-based controllers. In addition, hardware implementation methods will be investigated for the proposed control scheme, taking into account timing and resource consumption.

References

[1] J. P. M. Figueiredo, F. L. Tofoli and B. L. A. Silva, A review of single-phase PFC topologies based on the boost converter, 2010 9th IEEE/IAS International Conference on Industry Applications - INDUSCON 2010, Sao Paulo, Brazil, 2010, pp. 1-6

[2] K. B. Park, G. W. Moon and M. J. Youn, High Step-up Boost Converter Integrated With a Transformer-Assisted Auxiliary Circuit Employing Quasi-Resonant Operation, in IEEE Transactions on Power Electronics, vol. 27, no. 4, pp. 1974-1984, Apr. 2012.

[3] L. Schmitz, M. C. Orige, D. C. Martins and R. F. Coelho, High-Gain ZVS-ZCS DC-DC Landsman Converter With Low-Input Current Ripple, in IEEE Transactions on Industrial Electronics, vol. 71, no. 12, pp. 15835-15845, Dec. 2024.

[4] S. Kapat, and P. T. Krein, A tutorial and review discussion of modulation, control and tuning of high-performance dc-dc converters based on small-signal and large-signal approaches. IEEE Open Journal of Power Electronics, 1, 339-371, 20 Aug. 2020.

[5] B. Schwabe, A. Bach and T. Senjab, Interpretable AI for Power Conversion Control, 2023 IEEE Applied Power Electronics Conference and Exposition (APEC), Orlando, FL, USA, 2023, pp. 2851-2858.

[6] F.E. Cellier and E. Kofman, Continuous system simulation. Springer Science and Business Media, 2006, pp. 411-425.

[7] E. Reichensdörfer, J. Günther, K. Diepold, Recurrent Neural Networks for PID Auto-tuning, Technische Universität München, Lehrstuhl für Datenverarbeitung, Munich, 2017.

[8] J. G. Ziegler and N. Nichols, Optimum settings for automatic controllers, Journal of Dynamic Systems Measurement and Control, Transactions of the American society of mechanical engineers, 64(8), pp. 759-765, Nov. 1942.